Towards morphological thoracic EIT: Major signal sources correspond to respective organ locations in CT

Damien Ferrario, Bartłomiej Grychtol, Andy Adler, Josep Solà, Stephan H. Böhm and Marc Bodenstein

Abstract

Lung and cardiovascular monitoring applications of Electrical Impedance Tomography (EIT) require localization of relevant functional structures or organs of interest within the reconstructed images. We describe an algorithm for automatic detection of heart and lung regions in a time series of EIT images. Using EIT reconstruction based on anatomical models, candidate regions are identified in the frequency domain and image based classification techniques applied. The algorithm was validated on a set of simultaneously recorded EIT and CT data in pigs. In all cases, identified regions in EIT images corresponded to those manually segmented in the matched CT image. Results demonstrate the ability of EIT technology to reconstruct relevant impedance changes at their anatomical locations, provided that information about the thoracic boundary shape (and electrode positions) are used for reconstruction.

Index Terms

EIT, CT, shape, validation, localization

D. Ferrario and J. Solà are with CSEM – Centre Suisse d'Electronique et de Microtechnique, 2002 Neuchâtel, Switzerland, e-mail: dfr@csem.ch
B. Grychtol is with the German Cancer Research Centre (DKFZ), Department of Medical Physics in Radiology, 69120 Heidelberg, Germany
A. Adler is with Systems and Computer Engineering, Carleton University, Ottawa, ON K1S 5B6, Canada
S. Böhm is with Swisstom AG, 7302 Landquart, Switzerland
M. Bodenstein is with Department of Anesthesiology, Johannes Gutenberg-University Mainz, Mainz, Germany

Towards morphological thoracic EIT: Major signal sources correspond to respective organ locations in CT

I. INTRODUCTION

ELECTRICAL Impedance Tomography (EIT) is a medical imaging modality that allows recording of changes in the conductivity distribution within the body. Using a series of imperceptible current stimulations and voltage measurements from electrodes placed around the chest, EIT images of the thorax can be reconstructed. Cyclic air flow (respiration) within the lungs or blood filling of the heart and blood vessels modify the conductivity distribution of the thoracic cavity. A sequence of EIT images involving several cardiac and respiratory cycles represents such changes.

EIT has been demonstrated experimentally to represent regional ventilation (e.g. [9], [17], [21], [24]). This is of high clinical relevance, as EIT has the potential to become a routine means to identify optimal ventilator settings and thus help improve outcomes of mechanically ventilated patients. EIT is non invasive and can in principle be used for continuous monitoring.

However, despite its unique advantages and over two decades of research and development, EIT has not yet entered mainstream use in the intensive care unit. Clinical adoption is hindered by difficulties in analysing the EIT images caused, among others, by an uncertainty about the anatomical boundaries of the lungs on the reconstructed images and the source of the cardiac activity.

Several methods to segment the lung region of interest (ROI) in EIT images have been proposed. Using the standard deviation [14] or the maximum linear regression [16], images of the distribution of ventilation are computed. Thresholds then define ROIs with significant ventilation. Pulletz et al. [20] showed that both methods give similar results and have since often been used, with slight modification [11], [20]. However, since the most commonly used reconstruction algorithms produce EIT images that are circular, and thus do not correspond to the anatomy, none of these methods could be validated against a morphological medical imaging modality.

Isolating cardiac-related activity is more challenging, due to its smaller amplitude, the concurrent pulmonary and systemic perfusion and the potential overlapping with respiratory harmonics. Frerichs et al. [9] used breath holding to remove respiratory activity and electrocardiogram-gated-EIT [7]. Both techniques have been shown to correctly separate cardiac activity, but they need either the patient's engagement or additional equipment (ECG). Frequency-based [25] and statistics-based (PCA/SVD) algorithms [6] have then been used to identify cardiac changes. Pikkemaat et al. [19] compared both methods and obtained similar results. However, signals obtained with statistical-based algorithm are more complex to interpret [15].

Moreover, the exact underlying physiological mechanism of the EIT signal at cardiac frequencies remains unknown, with recent results indicating that impedance-pulsatility does not reflect lung perfusion [4]. One might hypothesize that the filling of heart chambers with blood generates a decrease in regional impedances. However, the mechanical interactions occurring at the heart-lung interface might also be a source of cardiac-related EIT signals.

In this paper, for the first time, functional EIT images are compared directly with the anatomy as seen on a CT slice in the plane of the electrodes. The sources of ventilation- and cardiac-related activity in the EIT images are localised by a novel unsupervised method combining statistical and spectral analysis with an image processing algorithm to find the heart rate and to define heart and lung ROIs. The comparison is facilitated by the recent enhancements to the EIDORS software allowing reconstruction of EIT images with arbitrary boundary shape.

II. METHODS

Overview: Simultaneous EIT data and CT images were acquired in pigs (section II-A), and CT slices within the EIT electrode plane were segmented to identify heart and lung regions (II-B). A finite element model (FEM) was created for each individual animal based on its own segmented CT scan. These were employed in a time difference EIT reconstruction algorithm to reconstruct the EIT image sequence (II-C). This temporal image sequence was analysed with a novel algorithm, which uses temporal and spatial information to detect and localize heart and lung regions (II-D). Finally, the detected functional regions within the EIT images were validated against the manually segmented CT images (II-E).

A. Experimental procedure

Experiments were conducted at the University of Mainz, Germany with appropriate ethical approval (licence no. 1.5 177-07/041-75, Landesuntersuchungsamt Rheinland-Pfalz, 56028 Koblenz, Germany). Experiments were carried out on 12 ± 3 weeks old pigs weighting 23 ± 2 kg. The animals were sedated by intramuscular injection of 8 mg/kg azaperon, 8 mg/kg ketamine and 0.2 mg/kg midazolam prior to transportation to the animal laboratory. General anesthesia was induced by 4 μg/kg fentanyl, 4 mg/kg propofol and 0.15 mg/kg pancuronium via peripheral intravenous injection. The pigs were intubated via the orotracheal route. They were ventilated with a standard clinical ventilator (AVEA,
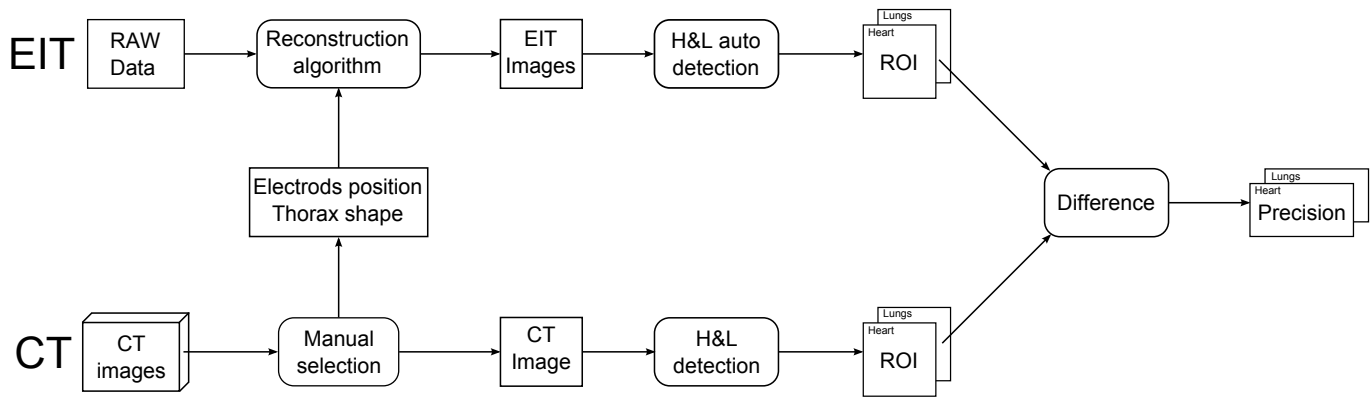
Fig. 1. Block diagram of the proposed method to compare regions of interest (ROI) of heart and lung activity as detected by EIT to ground-truth CT scan segmentation of these organs. In order to facilitate the comparison, EIT images were generated by using accurate position of EIT electrodes as extracted from CT images. The heart and lung (H&L) ROIs within the EIT images were then automatically identified and compared to the structures manually segmented in the CT images. Finally, the precision of the automatic identification was assessed.

CareFusion, San Diego, CA, USA) with a PEEP of 5 mbar, a FiO$_2$ of 0.5 and an I:E ratio of 1:1. General anesthesia was maintained by continuous intravenous administration of 15 mg/kg/h propofol and additional boluses of 4 µg/kg fentanyl (e.g. before surgery, before euthanasia). Canulation of right Vena jugularis interna (pulmonary artery catheter), one Vena femoralis (central venous access) and one Arteria femoralis (arterial catheter) were achieved by surgical cut-down of the respective vessels. After the experiment the pigs were euthanized in deep analgosedation by intravenous injection of 40 mmol potassium.

During the study, the piglets were investigated using static thoracic computed tomography (CT) of the whole lung (5 mm slices, HRCT: Somatotom Plus 4, Siemens, Erlangen, Germany) at continuous positive airway pressure (CPAP) during 25 s of apnea at CPAP levels of 5, 15 and 45 mbar with periods of standard ventilation maintaining the same positive end-expiratory pressure (PEEP) interposed between them. Simultaneously, EIT measurements were taken (Goe-MF II EIT device, CareFusion, San Diego, CA, USA) with a sampling frequency of 13 Hz controlled by MCFEIT study software (University of Göttingen, Germany). In all pigs, 16 EIT measurement electrodes (Blue sensor: BR-50-K, Ambu, Bad Nauheim, Germany) were attached around a transversal thoracic layer defining the area to be represented in the EIT slice. In the cranio-caudal axis the level of this measurement layer was defined by an area between sternum and first mamilla of the pigs. The fold of the axilla was the upper limitation of the ring of electrodes in each pig. In post mortem examinations the level of the electrode layer was found to be 35 mm or more cranial from the expiratory position of the diaphragm.

B. CT data segmentation

For each animal, the CT slice corresponding to the electrode positions was manually segmented by an expert to identify heart and lung regions. CT-based inclusion criteria for image segmentation were: 1) healthy subject, with no obvious pneumonia or lung collapse, and 2) EIT electrode level at a position

caudal to the maximum heart area in the CT. Of the nine instrumented animals, seven met these criteria. After identifying within the stack the transverse CT slice which contained the highest number of electrode markers (metallic center points of the gel EIT electrodes), the following structures were manually segmented within that slice: 1) outline of the piglet's outer body contour (boundary); 2) positions of electrodes; 3) heart and lungs; and 4) the descending aorta. If no marker could be identified for an electrode, the electrode position was defined as the geometric center of its visible part within the analyzed slice. To account for the inherent limitations of transverse CT cuts through oblique structures (partial volume effects) the heart was segmented as the maximum outer boundary encompassing pixels which could be attributed to the heart (adjacent slices were consulted in difficult cases). The same approach was taken when segmenting the lungs. This led, in some cases, to a degree of overlap between the heart and lung regions.

In general, a different CT slice was segmented for each CPAP level reflecting the movement of the electrode plane with respect to the tracheal carina.
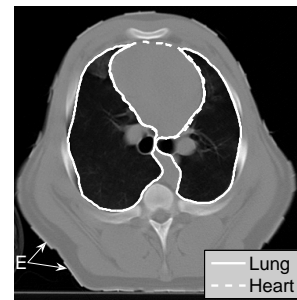

Fig. 2. Example of manual segmentation of the heart and lungs on a CT image of the electrode plane.

C. Morphological EIT image reconstruction

Using the boundary shapes segmented from CT, morphologically corresponding EIT images were reconstructed for each
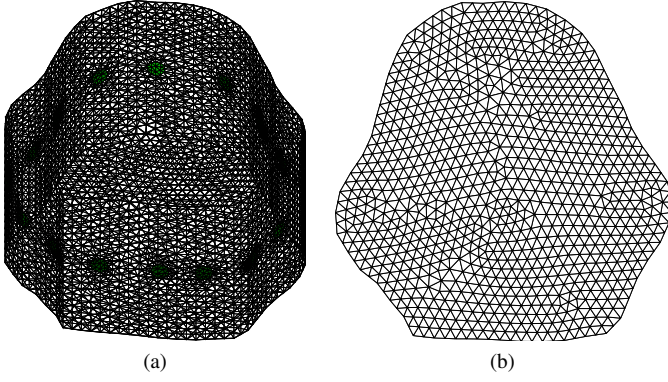
Fig. 3. Sample 3D fine (a) and 2D coarse (b) meshes used for forward and inverse modeling, respectively.

animal using EIDORS [3]. Normalized time difference EIT images of conductivity change were reconstructed from EIT measurements using a one-step Gauss Newton algorithm [2] which calculates a linear reconstruction matrix $\mathbf{R}$ that relates the calculated impedance image vector $\hat{\mathbf{x}}$ to the data vector $\mathbf{y}$ as:

$$\hat{\mathbf{x}} = \left(\mathbf{J}^t\mathbf{J} + \lambda\mathbf{P}\right)^{-1}\mathbf{J}^t\mathbf{y} = \mathbf{R}\mathbf{y} \qquad (1)$$

where $\mathbf{y} = \frac{\mathbf{v}}{\mathbf{v}_r} - 1$ is the normalized difference between a measurement $\mathbf{v}$ and the reference data $\mathbf{v}_r$. Here, the reference data set was chosen to be the mean EIT data over all frames; this choice has no effect on the properties of the EIT images in the frequency domain (except at DC). $\mathbf{J}$ is the Jacobian (or sensitivity) matrix of the forward model, and $\mathbf{P}$ is a Tikhonov type regularization matrix. $\mathbf{P}$ was formed from the sum of two parts: 1) the prior estimate of covariance between image elements (modeled as a Gaussian high pass filter using the approach of Adler and Guardo [2]), and 2) a model of the data variance due to electrode movement using the approach of Soleimani et al. [23]. Electrode movement compensation incorporates calculation of a *movement Jacobian* sensitive to linear displacements of each electrode, which, in our experience, significantly reduces image artifacts near the medium boundary. Noise variance was modeled to be equal on all EIT data channels, and the Tikhonov factor, λ, was chosen heuristically to give a good compromise between noise and image resolution.

To obtain accurate reconstructed object positions the 3D model used to calculate the forward model and the sensitivity matrix $\mathbf{J}$, and the 2D model on which the inverse solution was calculated were both conforming to the body shape as segmented from CT. The fine ($\sim 20 \times 10^3$ nodes) 3D forward model (Fig. 3a) was created using Netgen [22], an open-source meshing software, by extruding the boundary shape segmented from CT into the vertical direction by half the body width above and below the electrode plane. Electrodes were modeled at their exact and real anatomical positions using the complete electrode model [5] with FEM refinement in the region surrounding the electrodes. The coarse ($\sim 1 \times 10^3$ nodes) 2D FEM model (Fig. 3b) onto which EIT images were reconstructed was also built from the anatomical body shape, but without electrode refinement. Mapping between the

forward and inverse models was obtained by interpolating the area projected by the fine elements onto the coarse elements in the electrode plane.

EIT and CT image matching: Reconstructing EIT data on an anatomical model (rather than a circular one as is most often done) had a profound effect on the resultant images [13] and assured morphological correspondence between the EIT and CT images. To further facilitate comparison, the EIT images were interpolated from the original resolution of 32×32 pixels to match the resolution of the corresponding CT slices (originally 512×512 but cropped individually for each animal tightly around the shape), thus guaranteeing physical correspondence as well. A block diagram of the entire process allowing comparison between CT and EIT images is depicted in Fig. 4.
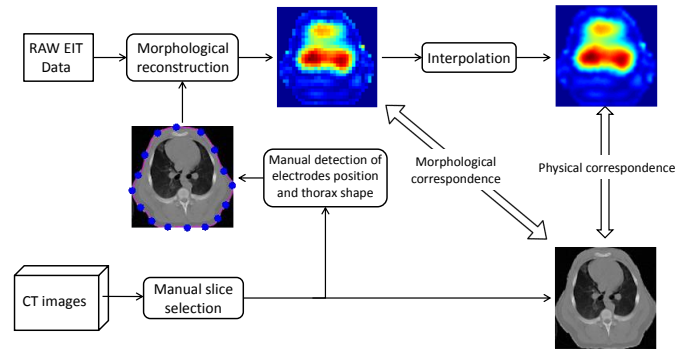

Fig. 4. Steps to obtain physical correspondence between EIT and CT images. Electrode position and thorax shape obtained from the CT image were used to reconstruct EIT images with the individual thoracic shape. EIT images were then interpolated to match the resolution of the CT images.

D. Unsupervised detection of lung and heart activity in EIT

Reconstructed EIT images were arranged in a matrix $\mathbf{x} \in \mathbb{R}^{I \times T}$ where I is the number of pixels in an image, and T the number of images (time points) in the series. From this sequence of images, regions containing significant cardiac and respiratory activity were automatically identified. Cardiac and respiratory frequencies were estimated and the amount of energy exhibited by each pixel at both frequencies was calculated resulting in functional images depicting cardiac and respiratory activity. Adjacent pixels with significant activity were identified and associated to the heart and lung regions of interest (ROI). An overview of the method is presented in Fig. 5. The method consisted of the following five steps A-E:

Step A — Filtering: A High Pass (HP) filter with a cutoff frequency of 0.05 Hz (4th order finite impulse response (FIR) filter) was applied to $\mathbf{x}$ along the time dimension to remove activity at low frequencies that was not related to heart or lung activity.

Step B — Respiratory frequency identification: The average signal m_1 was calculated as an ensemble average over pixels:

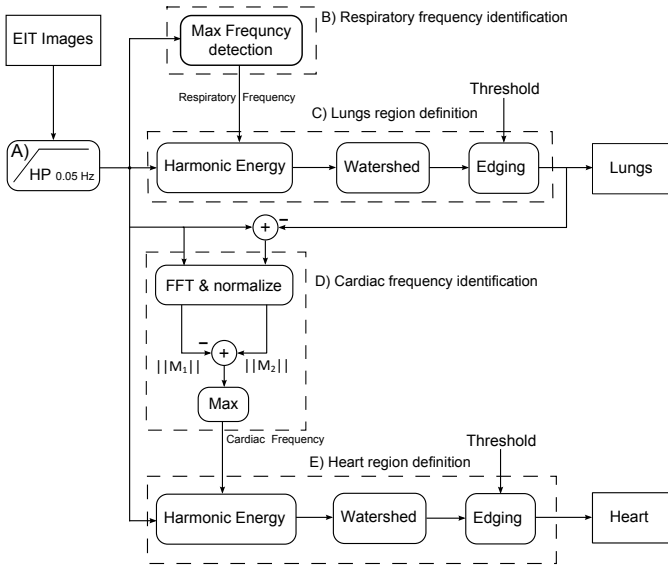$$m_1(t) = \frac{1}{I}\sum_{i=1}^{I} x_{i,t} \qquad (2)$$

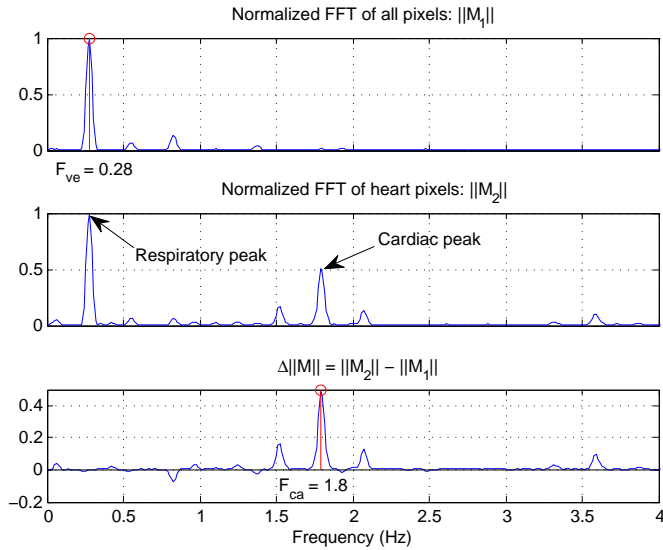Fig. 5. Block diagram of the automatic detection of the lungs and heart activity using EIT.

Fig. 6. Respiratory and cardiac frequency estimation. Top and middle figures illustrate the normalized FFT of respectively all EIT pixels and non-lung pixels. Peak frequency in the top figure is the respiratory rate. Cardiac rate is clearly amplified in the middle figure and remaining respiratory component canceled in the difference (bottom figure) allowing the detection of the cardiac frequency.

Respiratory frequency (f_{re}) was then determined as

$$M_1(f) = \mathcal{F}\{m_1(t)\} \tag{3}$$

$$f_{\mathrm{re}} = \arg\max_f |M_1(f)| \tag{4}$$

where $\mathcal{F}$ indicates the discrete Fourier transform (obtained through FFT). A sample frequency spectrum is presented in Fig. 6.

Step C — Lung region definition: Respiratory activity of each pixel was then calculated by estimating the actual energy at the respiratory frequency of pixel time series via a non-parametric periodogram approach.

The obtained image was interpreted as representing ventilation-related activity (Fig. 7, left). Regions containing the two strongest local maxima ($L_{\max 1}$, $L_{\max 2}$) were identified using the watershed technique [18] (Fig. 7, middle), and combined to form a lung ROI ($\mathrm{ROI_{Lung}}$), the size of which was controlled by an arbitrary threshold value $t_{\mathrm{Lungs}} \cdot L_{\max}$, where $0 \leq t_{\mathrm{Lungs}} \leq 1$ and $L_{\max}$ is the greater of $L_{\max 1}$ and $L_{\max 2}$. The greater the value t_{Lungs}, the more the resultant ROI focuses on the two peaks, treated as the source of the ventilation-related EIT activity. This effect is exemplified in Fig 8.
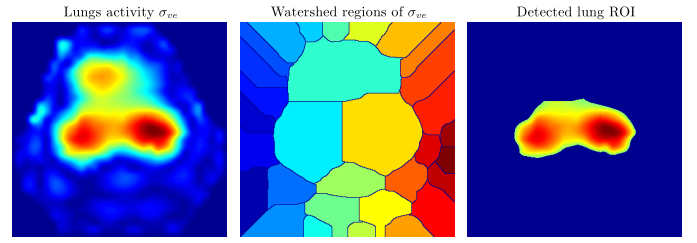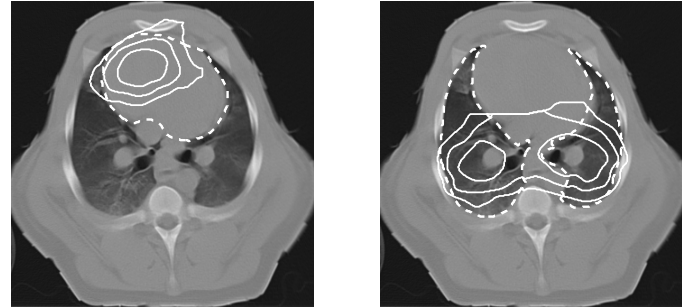
Fig. 7. Automatic identification of lung ROI in a sequence of EIT images. Left figure illustrates the distribution of energy at the respiratory frequency. Middle figure is the watershed of the energy image. Right figure shows the ROI with relevant respiratory activity identified as lung.

Fig. 8. Organ identification. Background: CT-scans of pig 1 at the level of the EIT electrodes at 5 mbar of PEEP. Dashed line ROIs were manually drawn and delineate heart and lungs. Automatically identified regions of cardiac and respiratory functional information are delineated by solid countour lines. Their respective areas show the influence of the automatic detection threshold. Threshold values were 0.25, 0.6 and 0.75 with 0.25 delivering the largest ROI.

Step D — cardiac frequency identification: Taking as $\mathbb{I}_2$ the set of $|\mathbb{I}_2|$ pixels that were not in the lung ROI as defined above with $t_{\mathrm{Lungs}} = 0.5$, the ensemble average m_2 was defined as

$$m_2(t) = \frac{1}{|\mathbb{I}_2|} \sum_{i \in \mathbb{I}_2} x_{i,t} \tag{5}$$

The signal $m_2(t)$ still contained some ventilation-related activity, but much less than $m_1(t)$. Accordingly, the spectral content of all the EIT images can be thought of as containing three components: respiratory M_{re}, cardiac M_{ca} and other organ activity or noise, grouped in M_η. The DFT of $m_1(t)$ and $m_2(t)$ can then be expressed as

$$M_1 = M_{\mathrm{re}} + M_{\mathrm{ca}} + M_\eta \tag{6}$$

$$M_2 = \alpha M_{\mathrm{re}} + \beta M_{\mathrm{ca}} + \gamma M_\eta \tag{7}$$
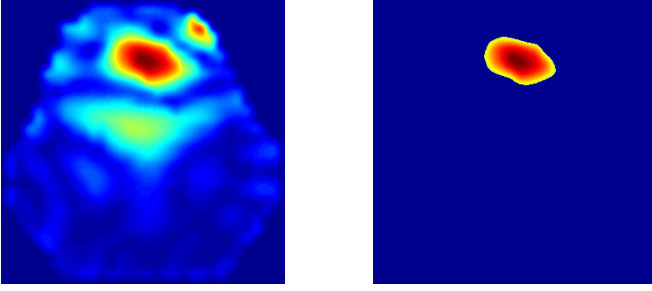
Fig. 9. Automatic detection of heart ROI in a sequence of EIT images. Left figure illustrates the distribution of energy at cardiac frequency and right figure the ROI with significant heart activity.

where the suppression factors $0 \leq \alpha, \beta, \gamma \leq 1$ account for the lost activity of the lung region excluded from $\mathbb{I}_2$. Because pixels exhibiting strong ventilation activity (ROI$_{\text{Lung}}$) were excluded from M_2, $\beta \geq \alpha$ (assuming heart and ventilation activity are not co-located). If noise is evenly distributed over the image, it will be attenuated at least as much as the ventilation activity, hence $\beta \geq \gamma$.

To yield an estimate of the cardiac frequency f_{ca} (Fig. 6), M_1 and M_2 were normalized with respect to the ventilator frequency:

$$\|M_1\| = aM_1 = a\left(M_{\text{re}} + M_{\text{ca}} + M_\eta\right) \tag{8}$$

$$\|M_2\| = bM_2 = b\left(\alpha M_{\text{re}} + \beta M_{\text{ca}} + \gamma M_\eta\right) \tag{9}$$

(a and b being normalization factors) and subsequently subtracted:

$$\begin{aligned}\Delta\|M\| &= \|M_2\| - \|M_1\| \\ &= (b\alpha - a)M_{re} + (b\beta - a)M_{\text{ca}} + (b\gamma - a)M_\eta\end{aligned} \tag{10}$$

In the difference $\Delta\|M\|$ between the normalized spectra, the energy in the respiratory band cancelled out ($b\alpha - a = 0$), whereas energy in the cardiac frequency band was preserved since respiration was more attenuated than cardiac activity in $M_2(\beta \geq \alpha)$, thus $b\beta - a > 0$. Finally, assuming cardiac energy to be larger than noise $M_{ca} > M_\eta$ and since $\beta \geq \gamma$, f_{ca} becomes the strongest component of $\Delta\|M\|$ (c.f. Fig. 6). This demonstration is independent of the cardiac and respiration frequency and the method should work even if the cardiac frequency were to coincide with a respiratory harmonic, as long as the fundamental respiratory frequency remains the strongest component of M_1 and the true $f_{ca} \neq f_{re}$.

Step E — Heart region definition: ROI$_{\text{Heart}}$ was defined analogously to ROI$_{\text{Lungs}}$. First, the energy of each pixel at the cardiac frequency was calculated to obtain an image representing the cardiac-related activity. Then, the same algorithm used to identify ROI$_{\text{Lungs}}$ (Step C) is applied but this time only the maximum of the image was taken as the center of the heart-related activity, and consequently a single watershed region was selected as ROI$_{\text{Heart}}$ (Fig. 9).

E. Assessment of morphological correctness of EIT

While EIT can neither be expected to reconstruct exact tissue boundaries nor produce anatomical images, it is nonetheless important that reconstructed impedance changes appear at anatomically meaningful positions, and that the geometrical relations between the different organs are preserved on EIT images, a property we call localization.

To measure the localization of the lung signal, we first define *precision* as the fraction of pixels in ROI$_{\text{Lung}}$ (obtained from the EIT recording as described in Step C above) that fall within the lung area (as segmented on CT)

$$precision = \frac{|\text{ROI}_{\text{Lung}} \cap \text{Lung}|}{|\text{ROI}_{\text{Lung}}|} .$$

Like the size of the ROI$_{\text{Lung}}$, *precision* depends on the value of the threshold t_{Lungs}. If the peak of ventilation activity L_{max} lies within the segmented lung area, *precision* is guaranteed to reach 100% for some value of t_{Lungs}. For each animal and pressure, we took the value of t_{Lungs} required to achieve *precision* of 50, 75 and 90 per cent as a measure of localization of the EIT signal. The smaller the value t_{Lungs} at which a given *precision* was achieved, the better localized the EIT signal was. We performed the same analysis for the heart ROI.

III. RESULTS

The *precision* of lung localization for each animal and PEEP level as a function of the t_{Lungs} threshold is presented in Fig. 10. In all cases, *precision* of 100% (i.e. 1) was reached, meaning that the maxima of respiratory activity derived from EIT recordings were always localized within the anatomical areas of the lungs as segmented from CT. The minimum t_{Lungs} values required to achieve the *precision* levels of 25, 50, 75 and 90 per cent are reported in Table I. Taking an average over all PEEP levels, 75% of pixels with just under half (0.4717) the maximum ventilation activity observed within an image (the "half-amplitude set" as defined in [1]) lie within the anatomical lung region. As evidenced by both Fig. 10 and Table I, the localization of lung activity in EIT varied within the same subject with the level of PEEP applied, thereby producing in general the best localization (higher precision for a given t_{Lungs} value in Fig. 10 and, conversely, a lower average t_{Lungs} for a given *precision* in Table I) at the highest pressure of 45 mbar. The only exception to this rule is pig 6 for which EIT *precision* was worst at 45 mbar (c.f. Fig. 10).

TABLE I
AVERAGE VALUE OF THE LUNG DETECTION THRESHOLD (t_{Lungs})
REQUIRED TO ACHIEVE A GIVEN *precision*

PEEP	*precision*			
[mbar]	25%	50%	75%	90%
5	0.0010	0.0066	0.6193	0.8691
15	0.0366	0.2506	0.5650	0.8464
45	0.0010	0.1223	0.2307	0.7229
all	**0.0129**	**0.1265**	**0.4717**	**0.8128**

t_{Lungs} is a unitless fraction adjusted between 0 and 1. Reported are averages over all animals for a given PEEP level (all levels in bold) of values required to achieve the respective *precision* value.
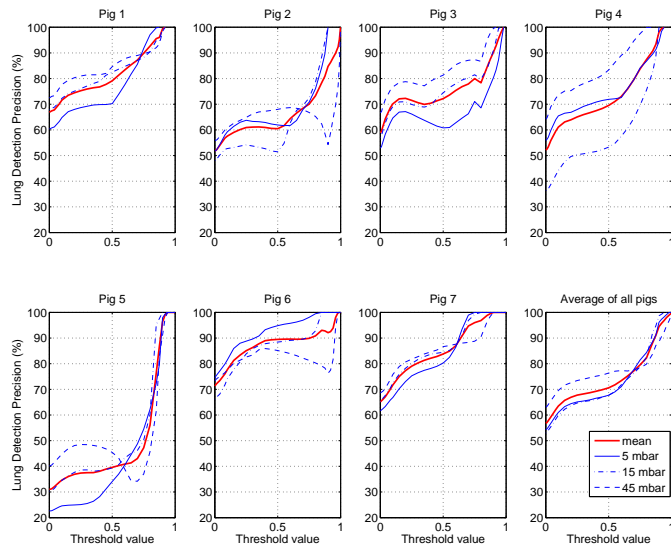
Fig. 10. Influence of the threshold t_{Lungs} on the *precision* of automatic detection of lungs ROIs in individual animals (aggregate results on bottom right). In general, and with the notable exception of pig 6, for a given value of t_{Lungs} higher *precision* was obtained at higher pressures.

Fig. 11. Influence of the threshold t_{Heart} on the *precision* of the EIT automatic detection of heart ROIs in individual animals (aggregate results on bottom right). With the exception of pig 2 at 5 mbar, 100% *precision* was achieved in all cases.

The maxima of cardiac activity within the EIT images were in all cases located within the heart as defined on the corresponding CT slice. As manifested by the increasing value of t_{Heart} required to achieve a given *precision* level (Table II), the heart activity seen in EIT was less locally confined at higher PEEP levels.

TABLE II
AVERAGE VALUE OF THE HEART DETECTION THRESHOLD (t_{Heart})
REQUIRED TO ACHIEVE A GIVEN *precision*

PEEP	*precision*			
[mbar]	25%	50%	75%	90%
5	0.0010	0.0010	0.1473	0.3214
15	0.0010	0.0366	0.2716	0.4500
45	0.0010	0.0010	0.2857	0.4643
all	**0.0010**	**0.0239**	**0.2349**	**0.4119**

t_{Heart} is a unitless fraction adjusted between 0 and 1. Reported are averages over all animals for a given PEEP level (all levels in bold) of values required to achieve the respective *precision* value.

IV. DISCUSSION

We compared EIT lung and heart regions of interest (ROI) detected by a novel unsupervised method during conventional ventilation at positive end-expiratory pressure (PEEP) levels of 5, 15 and 45 mbar against the area of the respective organs in the electrode plane as segmented from CT acquired at equal levels of positive airway pressure. The comparison was enabled by reconstructing EIT data using finite element models corresponding to the boundary shape of the thoracic surface, as opposed to cylindrical ones as is the standard practice. Images of heart and lung activity were obtained through a combination of spectral analysis and image processing techniques. For each image, the size of the ROI was controlled by a threshold expressed as a percentage of the highest value in the image.
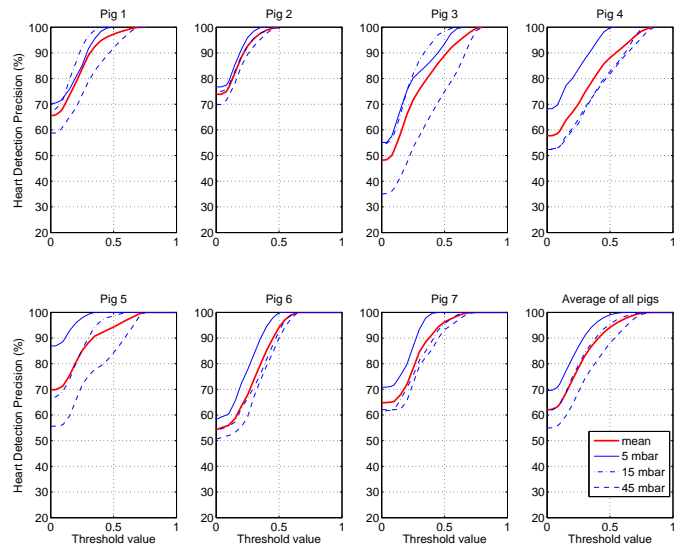
In all cases, the maxima of heart and lung activity as seen on EIT were within the respective organ as segmented from the corresponding CT image. At threshold values of, respectively, 47 and 23 per cent for t_{Heart} and t_{Lungs}, 75 per cent of lung and heart ROI overlapped with its true extent, demonstrating good localization of signals in EIT.

We found that the lungs are generally better localized at higher PEEP levels. We speculate that this is associated with a shift of ventilation-related activity in a dorsal and caudal direction with increasing PEEP, as reported in literature (e.g. [10]). On a typical CT slice, the area occupied by the lungs increases in the dorsal direction, with the features being finer in the ventral part. Due to the strong spatial smoothing inherent in EIT, the *precision* measure performs better when the focus of ventilation activity is more dorsal and thus more distant from the heart.
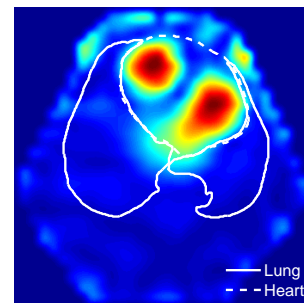

Fig. 12. Heart activity detected in Pig 2. The two peaks are opposite in phase. White lines delineate the organs as segmented from CT.

In one case, presented in Fig. 12, we noticed two clear foci of activity at the cardiac frequency in the EIT image, both contained within the heart region as segmented from CT. The cardiac-frequency activity at the two locations was opposite in phase and thus could represent the ventricles and the atria,

respectively. However, similar, sometimes multiple, opposite-phase peaks were subsequently found in other animals, e.g. the one presented in Fig. 9, but they were usually much weaker and located outside the heart area as segmented from CT. A similar phenomenon can be observed in the results reported in [26]. We therefore speculate that this effect is associated with the movement of the heart wall at the heart-lung interface. By comparing with ECG the phase of the weak cardiac frequency observed within the lung ROI (found to be delayed with respect to changes in the heart ROI), it has previously been demonstrated that they represent changes in blood volume [26]. However, the opposite-phase (rather than just delayed) features around the heart, and more specifically the very clear lines which separate them, have not so far been explored (to the best of the authors' knowledge) and may prove a useful feature for further improving the delineation of the heart within thoracic EIT images. In the future, we hope to develop a robust automatic detection of the heart that would take advantage of this effect.

In our analysis of the CT data, we observed that the CT slice that best represented the EIT electrode plane remained virtually fixed with respect to bony landmarks on the spine. However, the organ content and contours within the EIT plane of each animal varied significantly with CPAP levels as a result not only of the downward displacement of the diaphragm by up to 30 mm but also of the marked changes in the shape of the heart, which shortened along the cranio-caudal axis by up to 25 mm. The scale of these movements varied greatly between the animals. The observed positions of the heart, diaphragm, carina and the electrode plane at the different CPAP levels are presented as a boxplot in Fig. 13. This observation is potentially relevant for PEEP titration studies, most of which have thus far used the same EIT model and background conductivity throughout the experiment, ignoring the changes associated with organ movement. It remains to be investigated to what extent organ movement impacts the clinically relevant information contained within EIT images.

One limitation of our study is that we only used a single CT slice to compare against EIT images, while the electrode plane is rarely aligned with the CT slices. Moreover, electric current permeates a much larger volume of the body and hence tissue above and below the electrode plane affects the EIT measurements, much more than it does in CT. This limitation was most obvious in the calculation of *precision* for pig 6 in which the distance between the electrode plane and the diaphragm at 5 mbar was the smallest (20 mm). Consequently, the CT slice that contained the most electrodes at 5 mbar contained no tissue separating the two lungs which were therefore segmented together within a single ROI. At higher PEEP values, as the heart and the EIT plane moved upwards and the lungs moved downwards, the latter became easily separable in CT but not in EIT, where lungs usually appeared as a single ROI at all but the highest threshold values (cf. Fig. 8). This explains the observed decrease in *precision* with increasing pressure in this particular animal.

Another limitation inherent to our method is the use of a-priori information about the position of the electrodes and the thoracic shape which are hardly available at the bedside. Even
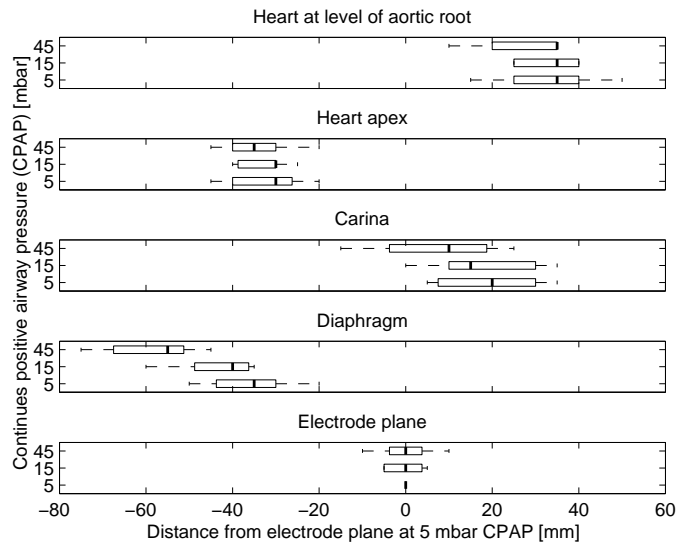

Fig. 13. Organ and electrode plane positions along the cranio-caudal axis for CPAP levels between 5 and 45 mbar. The centre of the uppermost costovertebral joint was used as anatomical point of reference but movements are referenced to the electrode plane as observed at 5 mbar. Negative numbers represent positions caudal to the electrode plane. Boxes show interquartile range with median indicated as a thick line, while whiskers show the range of data.

if recent findings highlight the importance of adequate information about the anatomical contour [13] and the electrode positions [27] for a meaningful image reconstruction, further work is necessary to quantify the influence of using accurate anatomical boundary shape and electrode positions for EIT reconstruction.

V. CONCLUSION

We presented a novel unsupervised method for defining heart and lung regions of interest in a sequence of EIT images and extracting the corresponding signals. The method allows for the specificity–sensitivity trade off to be adjusted according to need with a single threshold parameter.

Applying the method to a data set of simultaneously acquired EIT and CT data, we have found that EIT pixels with the strongest heart and lung signals as detected by our method were located within the anatomical boundaries of their respective organs as segmented on corresponding CT images. We therefore conclude that, contrary to the common treatment of EIT as a qualitative modality with poor anatomical correspondence, EIT images preserve basic geometric relations between organs and roughly correspond to the anatomy. This knowledge could be used to recognize and reject implausible EIT images and thus increase confidence in this technology. Two equally important features of our method are prerequisites: 1) reconstruction of EIT data on models with correct anatomical boundary shape and 2) detection of heart and lung activity using both spatial and temporal information contained in the EIT data sequence. For clinical practice, our findings pave the way towards a novel use of EIT technology based not only on the functional but also the anatomical information it provides.

ACKNOWLEDGMENTS

REFERENCES

[1] A. Adler, J. H. Arnold, R. Bayford *et al*, "GREIT: a unified approach to 2D linear EIT reconstruction of lung images" *Physiol. Meas.* 30:S35–55, 2009

[2] A. Adler and R. Guardo, "Electrical Impedance Tomography: Regularised Imaging and Contrast Detection" *IEEE T. Medical Imaging*, 15:170–179, 1996.

[3] A. Adler, W. R. B. Lionheart, "Uses and abuses of EIDORS: An extensible software base for EIT" *Physiol. Meas.* 27:S25–S42, 2006

[4] J. B. Borges, F. Suarez-Sipmann, S. H. Bohm *el al*, "Regional lung perfusion estimated by Electrical Impedance Tomography in a piglet model of lung collapse" *J. Appl. Phys.* Published online before print September 2011, doi: 10.1152/japplphysiol.01090.2010

[5] K.-S. Cheng, D. Isaacson, J. S. Newell and D. G. Gisser, "Electrode models for electric current computed tomography" *IEEE T. Biomed. Eng.*, 36:918–924, 1989.

[6] J. M. Deibele, H. Luepschen and S Leonhardt, "Dynamic separation of pulmonary and cardiac changes in electrical impedance tomography" *Physiol. Meas.*, 29:S1–S14, 2008.

[7] B.M. Eyboglu and B.H. Brown, "Methods of cardiac gating applied potential tomography". *Clin. Phys. Meas.* 9 Suppl A:43–48, 1988

[8] T. Facet, "An introduction to ROC analysis Pattern Recognition Letters", 27:861–874, 2005.

[9] I. Frerichs, J. Hinz, P. Herrmann *et al*, "Regional lung perfusion as determined by electrical impedance tomography in comparison with electron beam CT imaging.". *IEEE Transactions on Medical Imaging 2002* 21:646–652, 2002

[10] I. Frerichs, G. Schmitz, S. Pulletz *et al*, "Reproducibility of regional lung ventilation distribution determined by electrical impedance tomography during mechanical ventilation". *Physiol. Meas.* 28(7):S261–7., 2007

[11] C. A. Grant, T. Pham, J. Hough *et al*, "Measurement of ventilation and cardiac related impedance changes with electrical impedance tomography". *Critical Care* 15:R37, 2011

[12] B. Grychtol, G. K. Wolf, A. Adler and J. H. Arnold "Towards lung EIT image segmentation: Automatic classification of lung tissue state from analysis of EIT monitored recruitment manoeuvres". *Physiol. Meas.* 31:S31–43, 2010

[13] B. Grychtol, W. Lionheart, G. Wolf, M. Bodenstein, A. Adler "Impact of model shape mismatch on reconstruction quality in ElectricalImpedance Tomography ". *IEEE T. Medical Imaging*, In Press, 2012

[14] G. Hahn, I. Sipinkova, F. Baisch and G. Hellige G, "Changes in the thoracic impedance distribution under different ventilatory conditions", *Physiol. Meas.* 16:A161–73, 1995.

[15] N. Kerrouche, C. N. McLeod and W. R. B. Lionheart, "Time series of EIT chest images using singular value decomposition and Fourier transfor", *Physiol. Meas.* 22:147–157, 2001.

[16] G. Kühnel, G. Hahn, I. Frerichs *et al*, "Neue Verfahren zur Verbesserung der Abbildungsqualität bei funktionellen EIT-Tomogrammen der Lunge", *Biomed. Tech.* 42:213–4, 1997.

[17] P. W. Kunst, A. Vonk Noordegraaf, O. S. Hoekstra *et al*, "Ventilation and perfusion imaging by electrical impedance tomography: a comparison with radionuclide scanning", *Physiol. meas.* 19(4):481-90, 1998.

[18] F. Meyer, "Topographic distance and watershed lines". *Signal Processing* 38:113–125, 1994.

[19] R. Pikkemaat and S. Leonhardt, "Separation of ventilation and cardiac related signals within EIT-data streams" *J. Phys.: Conf. Series* 224:012028, 2010

[20] S. Pulletz, R. Huibert, H. R. van Genderingen *et al*, "Comparison of different methods to define regions of interest for evaluation of regional lung ventilation by EIT" *Physiol. Meas* 27:S115–S127, 2006.

[21] J. C. Richard, C. Pouzot, A. Gros *et al*, "Electrical impedance tomography compared to positron emission tomography for the measurement of regional lung ventilation: an experimental study" *Crit. Care* 13(3):R82, 2009.

[22] J. Schöberl, "NETGEN: An advancing front 2D/3Dmesh generator based on abstract rules" *Comput. Visual. Science* 1:41–52, 1997

[23] M. Soleimani, C. Gómez-Laberge and A. Adler, "Imaging of conductivity changes and electrode movement in EIT", *Physiol. Meas.* 27:S103–S113, 2006

[24] J. A. Victorino, J. B. Borges, V. N. Okamoto *et al*, "Imbalances in regional lung ventilation: a validation study on electrical impedance tomography", *Am. J. Resp. Crit. Care Med.* 169(7):791-800, 2004.

[25] M. Zadehkoochak, B H Blott, T K Hames and R F George "Pulmonary perfusion and ventricular ejection imaging by frequency domain filtering of EIT (electrical impedance tomography) images", *Clin. Physiol. Meas.* 13 Suppl A:191-6, 1992

[26] C. A. Grant, T. Pham, J. Hough, T. Riedel, C. Stocker, A. Schibler "Measurement of ventilation and cardiac related impedance changes with electrical impedance tomography", *Critical Care.* 15:R37, 2011

[27] J.A. Victorino, J.B. Borges, V.N. Okamoto, G.F.J. Matos, M.R. Tucci, M.P.R. Caramez, H. Tanaka, F. Suarez-Sipmann, D.C.B. Santos, C.S.V. Barbas, C.R.R. Carvalho, M.B.P. Amato. "Imbalances in Regional Lung Ventilation: A Validation Study on Electrical Impedance Tomography", *Am J Respir Crit Care Med* 169, 791-800, 2004

Damien Ferrario studied electronic engineering at the University of Applied Sciences of west Switzerland, and graduated in 2005. He pursued his academic career at Ecole Polytechnique Fédérale de Lausanne (EPFL), where he received his M.S. degree in electrical engineering in 2008.

He worked in the turbomachinery industry as embedded software engineer where he contributed to the design and implementation of signal processing algorithms for vibration monitoring. Since 2010, he is R&D engineer at the Systems Engineering Department of the Centre Suisse d'Electronique et de Microtechnique (CSEM) where he is involved in research and industrial projects in the fields of blood pressure, EIT, pulse oximetry (SpO2) and core body temperature.


Bartłomiej Grychtol received the B.S. degree in electrical engineering and computer science from Jacobs University, Bremen, Germany, in 2006 and the EngD degree in medical devices from University of Strathclyde, Glasgow, UK, in 2011.

In 2010-2011, he worked as a part-time Research Associate at the Department of Mathematics, University of Manchester, UK. Since 2010, he has been with the Department of Medical Physics in Radiology at the German Cancer Research Center (DKFZ), Heidelberg, Germany. His research interests include computer graphics, medical imaging, biomedical signal processing and artificial intelligence. Dr. Bartłomiej Grychtol received the Alexander von Humboldt Fellowship for Postdoctoral Researchers in 2011.

Andy Adler is professor and Canada Research Chair in biomedical engineering in Systems and Computer Engineering at Carleton University in Ottawa, Canada. His research interests are in: biometrics imaging and security systems, and the associated algorithms, measurement devices, and privacy and security aspects; and development of non-invasive biomedical measurement technologies and sensors, including the medical image and signal processing algorithms.
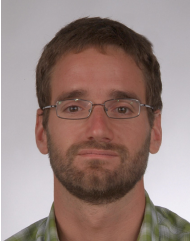
Josep Solà received his M.S. degree on Telecommunication Engineering from the Universitat Politècnica de Catalunya (UPC) after writing his master thesis within the R&D department of SONY International (Germany). In 2011 he received his PhD from the Eidgenössische Technische Hochschule Zürich (ETHZ) in the field of non-invasive blood pressure monitoring.

He joined the biomedical team at CSEM in 2004, where he is currently senior R&D engineer. His domains of expertise go from the development of high-level signal processing algorithms, to their embedded implementation in fixed-point microprocessors. Specialized on the monitoring of the human cardiovascular system, he is currently involved in research and industrial projects in the fields of blood pressure, cardiac output, pulse oximetry (SpO2) and energy expenditure.

Stephan H. Böhm is co-founder and medical director of Swisstom AG in Landquart, Switzerland, a start-up company developing innovative medical devices based on Electrical Impedance Tomography (EIT). Before he had been working in different functions for several companies including CSEM on products for intensive care medicine, anesthesia and on technologies for non-invasive monitoring of blood glucose and blood pressure.

Until 2003 he was a practicing anesthesiologist, intensive care and emergency physician with a decade of clinical experience. He is actively involved in clinical and experimental research projects with various teams around the world. As an inventor of several patents on different methods for monitoring and optimizing lung, heart and circulatory function he is also consultant for GE, Philips and was advising among other Siemens, Dixtal Brazil on how to develop innovative medical products and on new business strategies for structural changes from pure medical device manufacturers to service providers. Mr. Böhm is author of multiple peer reviewed publications and as a dedicated lecturer in command of the management, communication, language and computer skills required for product development, research, education, teaching, training and publishing.

Marc Bodenstein graduated from Medical School (Georg-August University of Goettingen, Germany) in 2001. He received his MD degree in 2002 at the same University (thesis: automatic error correction in electrical impedance tomography data).

He worked as a resident in anaesthesiology at Charité Campus Benjamin Franklin from 2001 to 2005, since 2005 he is a staff member of the Department of Anaesthesiology in the University Medical Center Mainz. He was research fellow from 2006 to 2007. Clinical fellowships were intensive care and emergency medicine. Since 2010 he is consultant of intensive care medicine. His research interests are acute respiratory failure, pathophysiology of mechanical ventilation and methods to detect cyclical recruitment of atelectasis.